

STABILITY ANALYSIS AND DESIGN OF TIME-STEPPING SCHEMES FOR GENERAL ELASTODYNAMIC BOUNDARY ELEMENT MODELS

A. PEIRCE

Department of Mathematics, University of British Columbia, Vancouver, BC, Canada

E. SIEBRITS

Development Engineer, Schlumberger Dowell Inc., Tulsa, OK, U.S.A.

SUMMARY

In the literature there is growing evidence of instabilities in standard time-stepping schemes to solve boundary integral elastodynamic models.^{1–3} However, there has been no theory to support scientists and engineers in assessing the stability of their boundary element algorithms or to help them with the design of new, more stable algorithms. In this paper we present a general framework for the analysis of the stability of any time-domain boundary element model. We illustrate how the stability theory can be used to assess the stability of existing boundary element models and how the insight gained from this analysis can be used to design more stable time-stepping schemes. In particular, we describe a new time-stepping procedure that we have developed, which has substantially enhanced stability characteristics and greater accuracy for the same computational effort. The new scheme, which we have called ‘the half-step scheme’, is shown to have substantially improved performance for the displacement discontinuity boundary element method commonly used to model dynamic fracture interaction and propagation.

KEY WORDS: numerical instability; elastodynamics; boundary elements; dynamic fracture

1. INTRODUCTION

There is considerable interest in the numerical solution of the elastodynamic equations in the geosciences, both for geological prospecting and for assessing the dynamic effects of stress waves on surface structures and excavations, excavation support, and fractures. Boundary element algorithms, in the form of the displacement discontinuity method, provide an efficient representation of geological features such as faults, parting planes, and cracks. Since the boundary element method only involves the discretization of the boundary of the domain and the fractures themselves, there is considerable potential for modelling dynamic fracture propagation numerically without having to re-mesh the domain at each growth increment as would be the case with finite element and finite difference methods.

Unfortunately, there is growing evidence of ‘intermittent numerical instabilities’ in boundary integral elastodynamic models. Mack² and Siebrits³ have both noted numerical instabilities in their Three-Dimensional (3D) and Two-Dimensional (TWO4D) displacement discontinuity codes, respectively. 3D uses linear in time and constant in space functional variation on flat rectangular elements. TWO4D uses linear in time, and either constant in space (‘constant/linear’) or linear in space (‘linear/linear’) functional variations on straight-line elements. Tian⁴ and Loken⁵ have both

also noted numerical instabilities in their two-(IBEM2) and three-dimensional (3DFS) fictitious stress codes, respectively. 3DFS uses linear in time and constant in space functional variations on flat rectangular elements. IBEM2 uses constant or linear in time and constant in space functional variation on straight-line elements. Tian's⁴ direct boundary element code (DBEM2), which uses linear in time and quadratic in space functional variations, also exhibits numerical instabilities.

The above codes all use analytic integrations in time and space. A more recently published direct boundary element code, QUADPLET,⁶ which uses quadratic spatial and linear temporal elements, and numerical integrations for the spatial integrals, also goes unstable, e.g., the problem in which the circumference of a circular cavity is suddenly loaded by a normal traction axisymmetrically,⁷ is clearly unstable by 2000 time steps. There are also other independent references made to unstable boundary element methods in the literature, e.g. Koller *et al.*⁸ had to resort to a penalized least-squares formulation in terms of a Tikhonov stabilizing functional to eliminate spurious numerical 'oscillations'. Andrews¹ modeled mixed-mode shear slip with a boundary integral approach, where the spatial convolutions were performed in the Fourier domain. He also notes the presence of 'oscillations' in almost all the boundary integral models he considered, and for which he found no solution.

We have used the term 'intermittent instabilities' because of the way in which the instabilities appear and disappear as the time step and spatial mesh parameters are changed. As an example of this type of instability, consider a fixed spatial discretization of a boundary integral model of a given elastodynamic problem, and allow the time step-size to change. The time-domain boundary element model can be unstable for a certain step-size and become stable if the step-size is *increased*. If the step-size is increased further, then the boundary element model may become unstable again. In addition, these instabilities may occur for certain problems and not for others depending on the specific geometry of the problem.

This intermittent instability is unacceptable, as one cannot provide coherent guidelines about the appropriate choice of time step. In order to be practical, we require an algorithm whose stability is assured provided the time step satisfies a relatively simple criterion. The Courant–Fredricks–Lewy (CFL) upper bound on the time step for explicit finite difference and finite element schemes provides an example of such a criterion in numerical analysis. Such criteria cannot, however, be applied directly to boundary element schemes as they are based on a different formulation and discretization of the original system of partial differential equations.

In the boundary element formulation of elastodynamic problems a time-domain approach or a frequency-domain approach can be used. In the latter approach, the time dependence of the problem is removed by taking a Laplace or Fourier transform in the time variable. The original hyperbolic partial differential equations are thereby reduced to a sequence of elliptic (steady-state) partial differential equations that need to be solved for each frequency. The boundary element method is then used to solve these elliptic problems. The time evolution of the original system is then obtained by taking the appropriate inverse Laplace or Fourier transforms of the solutions to the elliptic problems. The benefit of the frequency domain approach is the efficient way in which the expensive time convolutions are performed. However, one disadvantage of the frequency-domain approach is that localized non-linear phenomena such as slip on a fault or the effect of nonlinear material within a crack-like excavation cannot be modelled. In order to model these phenomena, a full space–time discretization of the boundary integral equations is required. We therefore restrict ourselves in this paper to the space–time formulation of the boundary element equations.

In this paper we make use of the stability analysis framework, established for model problems based on the equations of elastodynamics,⁹ to develop the necessary tools to analyse the stability

properties of any time-stepping boundary element method. Because of the potential for dynamic fracture modelling by means of the displacement discontinuity method, we use these stability analysis tools to investigate the sources of the instabilities in the displacement discontinuity method. This theory can also be used to explain the superior stability characteristics of the ε -scheme⁹ for elastodynamic problems. In addition, we show how the insight gained from the stability analysis can be used to develop a new time-stepping scheme with enhanced stability characteristics. The enhanced stability characteristics and improved accuracy of the so-called half-step scheme is clearly demonstrated by contrasting its performance with the Trapezoidal scheme which is commonly used in boundary element algorithms.

In Section 2 the BE equations of elastodynamics are summarized and the typical discretization procedure is described. In Section 3 we develop the necessary tools to analyse the stability of any discretized time-domain boundary element formulation. In Section 4 we use the stability analysis tools to analyse the ε -scheme and to design the new half-step scheme both of which have enhanced stability properties. We contrast the performance of the half-step scheme with the Trapezoidal scheme in numerical examples. In Section 5 we summarize the results and make some concluding remarks.

2. BOUNDARY ELEMENT EQUATIONS

2.1. Boundary integral formulations

The direct boundary integral equations¹⁰ are obtained by combining the dynamic reciprocal theorem with the appropriate fundamental solutions to the equations of elastodynamics. In the absence of body forces and given zero initial conditions, the direct boundary element equations are given by

$$u_k(\xi, t) = \int_S [U_{ik}(\mathbf{x}, t; \xi, 0) * t_i(\mathbf{x}, t) - T_{ikj}(\mathbf{x}, t; \xi, 0) n_j * u_i(\mathbf{x}, t)] dS(\mathbf{x}) \quad (1)$$

Here $U_{ik}(\mathbf{x}, t; \xi, 0)$ are the displacement components due to a unit impulse load applied at $t = 0$ and the corresponding stresses $T_{ijk}(\mathbf{x}, t; \xi, 0)$ are obtained by substituting these displacements directly into Hooke's law. The explicit expressions for these fundamental solutions are:

$$U_{ij} = \frac{1}{4\pi\rho} \left\{ \frac{\partial^2}{\partial x_i \partial x_j} \left[\frac{1}{r} \int_{r/c_1}^{r/c_2} \tau f(t - \tau) d\tau + \frac{1}{c_1} \int_0^{r/c_1} f(t - \tau) d\tau \right. \right. \\ \left. \left. - \frac{1}{c_2} \int_0^{r/c_2} f(t - \tau) d\tau \right] + \frac{\delta_{ij}}{rc_2^2} f\left(t - \frac{r}{c_2}\right) \right\} \quad (2)$$

$$T_{ijk} = - \left[\lambda \frac{\partial U_{lk}}{\partial \xi_l} \delta_{ij} + \mu \left(\frac{\partial U_{ik}}{\partial \xi_j} + \frac{\partial U_{jk}}{\partial \xi_i} \right) \right] \quad (3)$$

where \mathbf{x} is the receiver position, ξ is the source position, c_1 and c_2 are the compressional (P) and shear (S) wave speeds, respectively, and for the unit impulse we let $f(t) = \delta(t)$.

The indirect boundary element methods (i.e. the fictitious stress method and the displacement discontinuity method) can be obtained from the direct boundary element method by superimposing an interior problem and an exterior domain problem.³⁻⁵ By subtracting the equations for the interior

region from those for the exterior region, an equation similar to (1) is obtained in which the tractions t_i and displacements u_i are replaced by the jumps in traction and displacement across the boundary between the two regions. By requiring that the displacement jumps are zero across the interface, we obtain the fictitious stress method. The displacements and stresses for the fictitious stress method are given by

$$u_k(\mathbf{x}, t) = \int_S U_{ki}(\mathbf{x}, t; \xi, 0) * F_i(\xi, t) dS(\xi) \quad (4)$$

$$\sigma_{kj}(\mathbf{x}, t) = \int_S T_{kji}(\mathbf{x}, t; \xi, 0) * F_i(\xi, t) n_j dS(\xi) \quad (5)$$

where $F_i = t_i^+ - t_i^-$ are the traction jumps across the fictitious stress surface S.

Similarly, by requiring that the tractions are continuous across the interface, we obtain the displacement discontinuity method. The displacement and stress equations for the displacement discontinuity method are given by

$$u_k(\mathbf{x}, t) = \int_S T_{kij}(\mathbf{x}, t; \xi, 0) n_j * D_i(\xi, t) dS(\xi) \quad (6)$$

$$\sigma_{kl}(\mathbf{x}, t) = \int_S S_{kl ij}(\mathbf{x}, t; \xi, 0) n_j * D_i(\xi, t) dS(\xi) \quad (7)$$

where $D_i = u_i^+ - u_i^-$ are the displacement jumps across the displacement discontinuity surface S, and $S_{kl ij}$ is given by

$$S_{kl ij} = - \left[\lambda \frac{\partial T_{mij}}{\partial \xi_m} \delta_{kl} + \mu \left(\frac{\partial T_{kij}}{\partial \xi_l} + \frac{\partial T_{lij}}{\partial \xi_k} \right) \right] \quad (8)$$

2.2. Discretization of the boundary integrals

The boundary integrals in the above equations contain two types of integrals, viz. time and space. The time integrals (embodied in the time convolution operator) are discretized into time steps, with a particular functional variation over each time step (e.g. constant, linear, etc.). The spatial boundaries are also discretized into elements. Each element is assumed to have certain geometric properties (e.g. straight or curved elements) and the functional variation over each element is assumed to be of a particular order (e.g. constant, linear, quadratic, etc.). The temporal integrals can all be performed analytically, and this is well documented.²⁻⁵ The spatial integrations are often determined numerically (e.g. Reference 11), especially in the case of higher-order geometrical and functional variations over each element. In the case where each element is assumed to be straight (or flat), these integrals can also be determined analytically.²⁻⁵

The time integrals in the boundary integral equations are discretized using techniques that are closely related to the methods commonly used to solve ordinary differential equations. In Appendix I the essential differences between these two classes of numerical problem are described.

There are restrictions governing the choice of functional variation in space and time. For example, in the displacement discontinuity method, a piecewise constant functional variation in time (in two and three dimensions) is not possible because it leads to infinite stresses at the wave fronts.^{2,3,5} Hence, a minimum requirement of the displacement discontinuity method is a linear

variation within each time step, with continuity between time steps. Furthermore, stability and accuracy considerations govern which orders of time and space functional variations are permissible, as will be seen later.

2.2.1. Temporal integrations. Assuming a piecewise linear time variation for the approximating function, denoted by $f(t)$, the integrations can be performed for the special case $f(t) = t/\Delta t$, and then generalized by combining three such staggered functions to obtain a ‘hat’ function, from which the piecewise linear time variation can be constructed. Hence,

$$f(t_k) = \left[H(t - t_{k-1}) \frac{\tau_{k-1}}{\Delta t} - 2H(t - t_k) \frac{\tau_k}{\Delta t} + H(t - t_{k+1}) \frac{\tau_{k+1}}{\Delta t} \right] \quad (9)$$

where $t_k = k \Delta t$ and $\tau_k = t - t_k$. The above approach is possible because of the linearity of the boundary element method (so that the principle of superposition applies), and because of the time translation property of all the fundamental solutions. Combining a hat function at each time step results in a piecewise linear temporal variation.²⁻⁵ Piecewise constant time elements can be constructed in a similar way, by combining three sets of Heaviside functions appropriately. Higher order in time variations can also be constructed, but are not covered here.

2.2.2. Spatial integrations. In the two-dimensional case, if we assume that the elements are straight-line segments, then analytic integrations are possible for functional variations that are constant, linear or quadratic along the element. This has been fully covered in References 4 and 3, and will not be repeated here. In the three-dimensional case, if we assume that each element is flat, then analytic integrations are once again possible.^{2,5} Alternatively, numerical integration procedures can be used. Care must be taken, especially in the displacement discontinuity element method, to avoid numerical problems with singularities at element edges because of the hypersingularity of the fundamental solutions of this method. In fact, the hypersingular nature of the stress equations for the displacement discontinuity method precludes the use of numerical integration schemes. Furthermore, element integrations must be causal (i.e. partial integrations are performed for those portions of the elements that fall within the causal space-time ‘light cone’) in order to ensure accurate influence coefficient calculations.

2.2.3. Numerical implementation. The discretization of the time and space integrals in any of the time-domain direct or indirect boundary element methods leads to a system of time marching algebraic equations of the form:

$$\mathbf{b}_m = \mathbf{C}_0 \mathbf{F}_m + \sum_{k=1}^{m-1} \mathbf{C}_{m-k} \mathbf{F}_k \quad (10)$$

where \mathbf{F} is the vector of unknown boundary tractions and/or displacements, or fictitious stresses, or displacement discontinuities, \mathbf{C}_k is the influence coefficient matrix, \mathbf{b} the boundary displacement and/or traction vector and m the current time step number.

In general, the matrices \mathbf{C}_k are fully populated. It is clear that the unknown quantities \mathbf{F}_m at the current time step m are obtained via a convolution between the known coefficients and known quantities from *all* previous times (in the two-dimensional case).

Algorithm (10) can be explicit (\mathbf{C}_0 diagonal) or implicit (\mathbf{C}_0 not diagonal), depending on the type of discretization that is used. If the functional variation is constant across an element, then the algorithm can be made explicit by choosing a small enough time step, in which case the

dimensionless mesh parameter $Q1 = c_1 \Delta t / \Delta x$ satisfies the inequality $Q1 < 0.5$. Here Δx is the element size and Δt is the size of the time step. In other words, the system is explicit if the compressional wave front travels less than half an element length in one time step. Of course, this pre-supposes that neighbouring elements are not at acute angles to each other, or closer than half an element length. In such cases, the time step restriction is more severe. If the functional variation over each element is variable, then the algorithm will always be implicit, because multiple collocation points within each element ensure that cross-coupling occurs regardless of the size of the time step, and hence the matrix \mathbf{C}_0 is never diagonal.

The stability of the algorithm is not guaranteed if the time step is chosen such that the scheme becomes implicit. This has to be tested, and will be shown later to depend on the functional variations across time steps and space elements as well as the geometric distribution of elements.

3. GENERALIZED STABILITY ANALYSIS

In this section we generalize the stability analysis which was developed in Reference 9 so that it can be applied to general boundary element formulations which reduce to the form (10). Because of the uniform spatial discretization of the one-dimensional wave model considered in Reference 9, it was possible to use the lattice Fourier transform to simplify the analysis considerably. Unfortunately, such simplification is not possible for general boundary element models so we need to develop the theoretical tools necessary to analyse the stability of matrix time-marching equations (10) directly.

3.1. The matrix stability problem

As a starting point we take the z -transform (see Reference 12, 13 and Appendix II) of the matrix equation (10) to obtain

$$\mathbf{b}(z) = \mathbf{C}(z)\mathbf{F}(z) \quad (11)$$

where the z -transforms of the vector and matrix sequences $\{\mathbf{b}_k\}$, $\{\mathbf{F}_k\}$, and $\{\mathbf{C}_k\}$ are defined in terms of the z -transforms of their components. For example,

$$\mathbf{C}(z) = [c_{ij}(z)] = \left[\sum_0^{\infty} [c_{ij}]_k z^{-k} \right] \quad (12)$$

In a typical boundary element problem we are given $\{\mathbf{b}_m\}$ and need to determine $\{\mathbf{F}_k\}$ and we represent this process in terms of (12) as follows:

$$\mathbf{F}(z) = \mathbf{C}^{-1}(z)\mathbf{b}(z) \quad (13)$$

The sequence $\{\mathbf{F}_k\}$ can now be represented using the inversion formula (33) and the adjoint formula for the inverse of a matrix

$$\mathbf{F}_k = \frac{1}{2\pi i} \int_C \left\{ \frac{\text{adj}(\mathbf{C}(z))}{\det(\mathbf{C}(z))} \mathbf{b}(z) \right\} z^{k-1} dz \quad (14)$$

where C is a contour that encloses all the poles of the expression between parentheses in (14). The poles that are due to the numerical scheme are determined by the zeros of the following equation:

$$\det(\mathbf{C}(z)) = 0 \quad (15)$$

The time-marching scheme is said to be stable⁹ if all the zeros of (15) lie within the unit disc. We therefore need to locate the zeros of (15) in order to be able to determine if a given discretization is stable. Our problem is that each of the elements of $\mathbf{C}(z)$ is an infinite series so that (15) potentially has an infinite number of roots.

3.2. Stability polynomials and the Argument principle

For problems in which the boundary elements are located within a finite region, the coefficient matrices $\{\mathbf{C}_k\}$ decay as $k \rightarrow \infty$. We can therefore approximate the infinite series $c_{ij}(z)$ by polynomials of degree at most M , which is sufficiently large for the dominant element-to-element influences to be included. Provided the truncated matrices are sufficiently small, the roots that are discarded by this truncation procedure will be close to zero and will not affect the stability analysis (see Appendix III). For an N degree of freedom boundary element model the \mathbf{C}_k are $N \times N$ matrices so that $\det(\mathbf{C}(z))$ is approximated by a polynomial of degree MN which we denote by

$$P_{MN}(z) = \det(\mathbf{C}_M(z)) \approx \det(\mathbf{C}(z)) \quad (16)$$

For large boundary element models (e.g. $N = 100$) with truncations involving even a modest number of time steps $M = 50$ we are faced with the problem of locating the roots of a 5000 degree polynomial. It is impracticable to determine explicit expressions for such high degree polynomials and finding such a large number of roots explicitly is computationally prohibitive. Our strategy will be to use the fact that we are trying to find the roots of an analytic function $P_{MN}(z)$ and concentrate on only those roots that can cause instabilities.

By means of the transformation $w = \frac{1}{z}$ the unstable roots $|z| > 1$ can be mapped into the unit disc. We therefore define the complimentary stability polynomial

$$Q_{MN}(z) = z^{MN} P_{MN} \left(\frac{1}{z} \right) \quad (17)$$

which has roots z_k inside the unit disc that correspond to the unstable roots of $P_{MN}(z)$ that fall outside the unit disc. Since $Q_{MN}(z)$ is an analytic function in the finite complex plane, the Argument principle^{14,15} implies that the number of roots of $Q_{MN}(z)$ contained within a closed curve C is given by the change in argument $(1/2\pi)\Delta\arg(Q_{MN}(z))|_{z \in C}$, which is an integer representing the number of times the point $w = Q_{MN}(z)$ winds around the origin as z traverses the curve C in a positive direction. In particular, if the curve is a circle C_r of radius r then the number of roots of $Q_{MN}(z)$ within the circle is given by $\frac{1}{2\pi}[\arg(Q_{MN}(re^{2\pi i})) - \arg(Q_{MN}(re^{0i}))]$. If we set $r = 1$ then $(1/2\pi)[\arg(Q_{MN}(e^{2\pi i})) - \arg(Q_{MN}(e^{0i}))]$ is the number of unstable zeros for the discretization. The application of the Argument principle thus enables us to ascertain the stability of a particular discretization by focusing on the number of unstable roots rather than having to determine all the roots.

Figure 1 shows a two-element displacement discontinuity model which served as a rather exacting test problem for stability. By varying the inter-element distance h it was possible to see the type of intermittent instabilities that have been reported in the literature. Figure 2 shows stability information for an unstable constant/linear two-element displacement discontinuity model. The first plot shows the image curve $Q(z)$ as the point z traverses the unit circle C_1 , the second plot shows the cumulative argument $\arg(Q(z = e^{i\theta}))$ for $0 \leq \theta \leq 2\pi$. Figure 3 shows the actual distribution of roots of $P(z)$ for the model. The cumulative argument plot predicts that there is one unstable root which is consistent with the diagram of the roots of the stability polynomial that are evaluated explicitly in this special case.

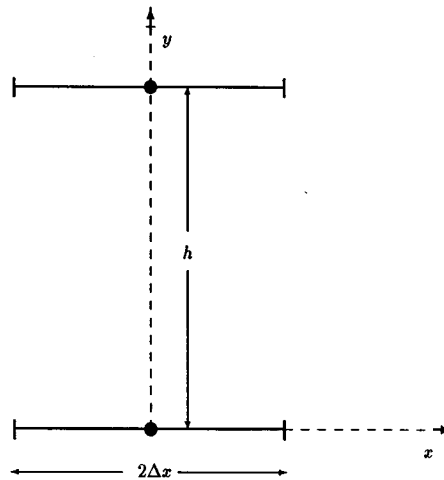


Figure 1. Two element problem geometry which exhibits instabilities

3.3. Implementation of the stability criterion

For large boundary element models even applying the stability criterion can become prohibitive. In this section we discuss some of the numerical techniques that can be used to make the stability checking more efficient.

3.3.1. Practical implementation of the Argument principle. The most expensive component in the stability criterion based on the Argument principle is the process of evaluating the complementary stability polynomial for various values of z along the boundary of the unit disc. The first step in evaluating $Q_{MN}(z)$ is to evaluate the truncated matrix polynomial $\mathbf{C}_M(z) = [\sum_{k=0}^M [c_{ij}]_k z^k]$. Since each coefficient in this matrix is a polynomial of degree M it is important to evaluate each of them efficiently using Horner's rule.¹⁶ In addition, in order to prevent the numbers from becoming too large in the evaluation of the polynomial and later in the evaluation of the determinant, the coefficients are scaled by dividing each of them by the largest matrix element $[c_{ij}]_k$ —typically the self-effect $[c_{ii}]_0$. The second step is to evaluate the determinant of the $N \times N$ matrix $\mathbf{C}_M(z)$ by performing an LU decomposition and then taking the product of the diagonal elements on the upper diagonal matrix. To avoid round-off errors for large boundary element models, this product can be performed by summing the logarithms of the diagonal elements. The complex argument of the determinant that we require for the Argument principle can be found by taking the imaginary part of the logarithm of the determinant, i.e. if $\det(Q_{MN}(z)) = \text{Re}^{i\Theta}$ then $\Theta = \text{Im}(\log(\det(Q_{MN}(z))))$.

Once we have a technique to evaluate the determinant $Q_{MN}(z)$ the next step is to find the cumulative argument $\bar{\Theta}$ of $Q_{MN}(z)$ as $z = re^{i\theta}$ traverses the stability circle. In order to achieve this we use the following procedure arg in which the determinant $\det(Q_{MN}(e^{i\theta_i}))$, the cumulative argument $\bar{\Theta}_i$ from the i th step, and the value of the determinant $\det(Q_{MN}(e^{i\theta_{i+1}}))$ at the $(i+1)$ th step are used to find the $(i+1)$ th cumulative argument $\bar{\Theta}_{i+1}$. The cumulative argument $\bar{\Theta}_i$ should be distinguished from the principal argument of $\det(Q_{MN}(e^{i\theta_i}))$ which is evaluated on the principal branch of the Riemann sheet and denoted by $\Theta_i = \text{Arg}(\det(Q_{MN}(e^{i\theta_i})))$. In the procedure that

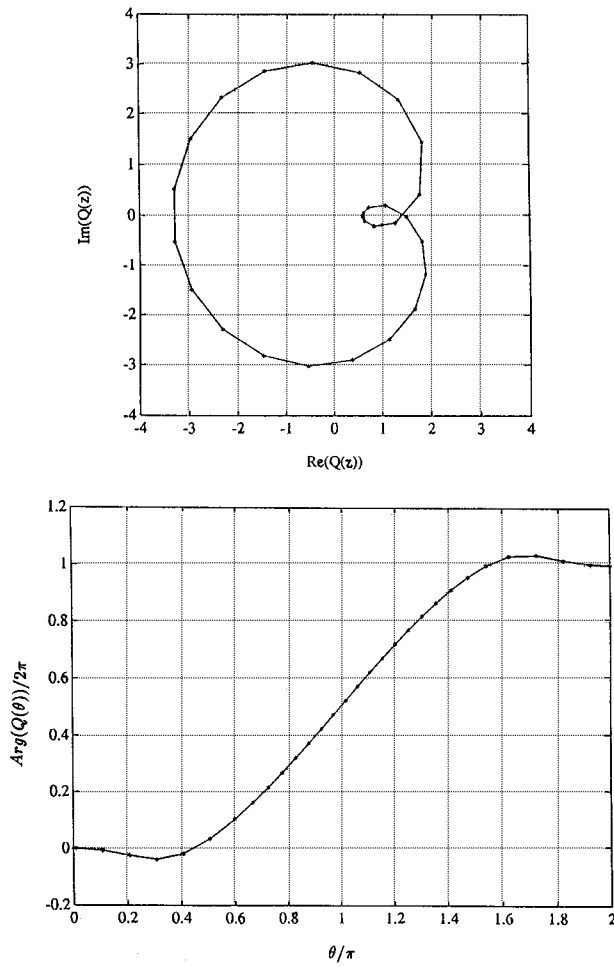


Figure 2. The image curve $Q(C_1)$ of the unit circle, and the cumulative argument $\arg(Q(z))$ for the unstable two-element displacement discontinuity model: (top) stability polynomial $Q(z)$ as z traverses the unit disk, (bottom) cumulative argument

follows we use the notation $[t]$ to denote the integer just less than t .

```

FUNCTION arg:  $\bar{\Theta}_{i+1} = \arg(\det(\theta_i), \bar{\Theta}_i, \det(\theta_{i+1}))$ 
 $\mathcal{N} = \text{sign}(\bar{\Theta}_i)[\bar{\Theta}_i/2\pi]$ 
 $\Theta_{i+1} = \text{Arg}(\det(\theta_{i+1}))$ 
if  $|\Theta_{i+1} - (\bar{\Theta}_i - \mathcal{N}2\pi)| > \pi$ 
 $\bar{\Theta}_{i+1} = (\mathcal{N} + \text{sign}(\bar{\Theta}_i))2\pi + \Theta_{i+1}$ 
else
 $\bar{\Theta}_{i+1} = \mathcal{N}2\pi + \Theta_{i+1}$ 
end if
end
    
```

where the shorthand notation $\det(\theta_i)$ has been used for the quantity $\det(Q_{MN}(e^{i\theta_i}))$.

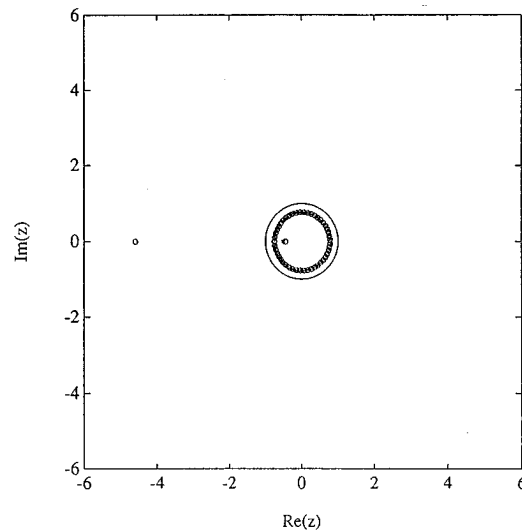


Figure 3. The actual distribution of roots of $P(z)$ for the two element problem

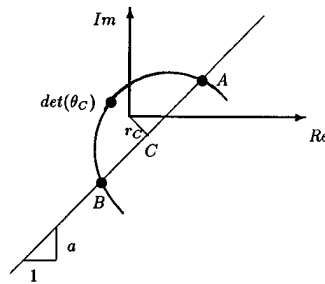


Figure 4. The situation representing a close shave of the origin by the points A and B

3.3.2. An adaptive algorithm to sample the stability boundary. When the Argument principle is applied, the sample rate of the stability circle can crucially affect the results as well as the efficiency of the algorithm. If the partition of the stability boundary is too coarse then we may miss some crucial loop around the origin. In contrast a very dense partition of the stability boundary will make it extremely expensive to evaluate the large number of determinants. We have developed an adaptive sampling procedure which adjusts the sampling density to make the changes in the cumulative argument $\bar{\Theta}$ roughly constant from one step to the next. In addition, logic is inserted to detect a situation in which the determinant makes a close shave to the origin in which case the sample density is increased to determine which side of the origin the determinant trajectory falls.

At the i th step the basis for choosing the sampling point at the $(i+1)$ th step is the gradient $d\bar{\Theta}/d\theta$ of the cumulative argument curve over the previous step. The formula we use for determining the $(i+1)$ th sampling point θ_{i+1} is as follows:

$$\theta_{i+1} = \theta_i + \Delta\bar{\Theta}_{\text{MAX}} \frac{(\theta_i - \theta_{i-1})}{(\bar{\Theta}_i - \bar{\Theta}_{i-1})} \quad (18)$$

where $\Delta\bar{\Theta}_{\text{MAX}}$ is the maximum change allowed in the cumulative argument $\bar{\Theta}$.

The criterion for determining a close shave is based on the orthogonal projection from the origin O to the closest point C on the line joining the point $A = \det(Q_{MN}(e^{i\theta_i}))$ and the point $B = \det(Q_{MN}(e^{i\theta_{i+1}}))$. If C falls on the line between A and B , and $OC \ll \min[|A|, |B|]$ then an additional sample-point is added at

$$\theta_C = \theta_A + \frac{\operatorname{Re}(C) - \operatorname{Re}(A)}{\operatorname{Re}(B) - \operatorname{Re}(A)}(\theta_B - \theta_A) \quad (19)$$

in order to determine whether the current loop includes the origin. The following procedure summarizes the logic to check for a close shave between two points A and B (also see Figure 4)

FUNCTION close: $(\theta_C, \text{flag}) = \text{close}(A, B, \theta_A, \theta_B)$

$$a = \frac{\operatorname{Im}(B) - \operatorname{Im}(A)}{\operatorname{Re}(B) - \operatorname{Re}(A)}, \quad b = \operatorname{Im}(A) - a \operatorname{Re}(A)$$

$$r_C = \frac{|b|}{\sqrt{1+a^2}}$$

$$\operatorname{Re}(C) = \frac{-ab}{1+a^2}$$

$$\theta_C = \theta_A + \frac{\operatorname{Re}(C) - \operatorname{Re}(A)}{\operatorname{Re}(B) - \operatorname{Re}(A)}(\theta_B - \theta_A)$$

$$\text{flag} = 0$$

$$\text{if } C \in \overline{AB} \text{ and } r_C < 0.2 \min[|A|, |B|] \text{ then flag} = 1$$

end

Once a close shave has been detected and a new sample point identified, the close shave procedure can be repeated until it is certain that the current values of the determinant are clear of the origin.

4. DESIGN AND PERFORMANCE OF NEW TIME-STEPPING SCHEMES

4.1. The two-element model, persistent wave fronts and stability

One of the trends that comes out of the analysis in Reference 9 is that the magnitude of the self-effect relative to those of the other element-to-element influences plays a crucial role in determining the stability of the time-stepping algorithm. The self-effect is the influence an element or collocation point has on itself in the first time step whereas the influence an element has on itself at a later time or the effect that an element has on one of its neighbours are referred to as 'other effects'. In the particular case of the one-dimensional wave model problem, the Trapezoidal constant/linear approximation is unstable. This instability is largely due to the fact that the kernel $H(x \pm ct)$ for the one-dimensional wave equation⁹ does not decay in space or time, so that the self-effect does not dominate the other element-to-element influences. The two-dimensional influence kernels do generally decay with space and time (see for example Reference 3). However, exceptions to the space-time decay for two-dimensional elastodynamic problems do occur for certain types of persistent solutions such as those for pressurized cracks (see Reference 17) and the stress waves that propagate along the axis of symmetry that lies perpendicular to displacement discontinuity elements. In this subsection we describe the persistent wave fronts for displacement discontinuity elements, demonstrate the diffraction effects from the corners of the elements, and discuss the influence this has on stability of the standard Trapezoidal time-stepping scheme.

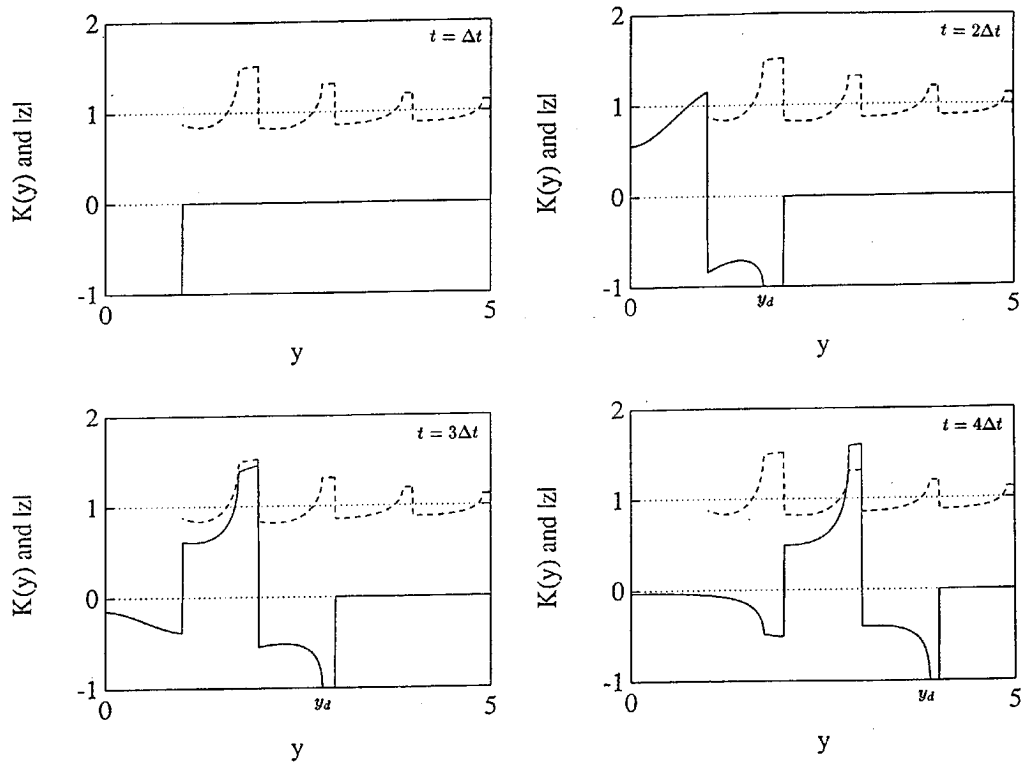


Figure 5. The stress response of a constant displacement discontinuity element along its center-line when it is subjected to triangular time pulses (solid), and largest root of the stability polynomial as a function of separation of the two element problem (dashed)

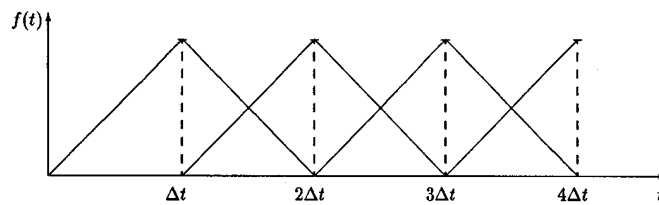


Figure 6. Basis functions for the trapezoidal/standard linear scheme

For simplicity we consider the displacement discontinuity method for antiplane motion and elements which have a piecewise constant spatial variation and piecewise linear time variation. In Figure 5 we show the spatial plots, observed at times $t = \Delta t$, $2\Delta t$, $3\Delta t$, and $4\Delta t$ along the element centre-line, of the wave fronts emanating from a displacement discontinuity element. In this figure, we have chosen $Q2 = c_2\Delta t/\Delta x = 0.5$, $E = 7.5398$ Pa, $\rho = \pi$ kg/m³, $\nu = 0.2$, and $\Delta x = 2$ m, which implies a shear wave velocity of $c_2 = 1$ m/s. The displacement discontinuity element has been excited by the Trapezoidal triangular hat functions that act initially over one time interval and subsequently over two time intervals as shown in Figure 6. In the first snap-shot in

Figure 5 at time $t = \Delta t$ the response to the triangular excitation of the displacement discontinuity element is a square-wave stress pulse $H(t - \Delta t) - H(t)$ that does not decay with distance. In the second snap-shot, observed at time $t = 2\Delta t$, the response is no longer a square-wave stress pulse but a perturbation of the pulse $H(t) - 2H(t - \Delta t) + H(t - 2\Delta t)$. The perturbation of this pulse results from the diffraction pulses that arrive at y_d from the edges of the element. To the left of this point y_d the pulse $H(t) - 2H(t - \Delta t) + H(t - 2\Delta t)$ is subjected to interference while to the right of y_d the pulse is undisturbed. In the third snap-shot, observed at time $t = 3\Delta t$, a similar diffraction-interference pattern is observed. In this case the response is a perturbation of the pulse $H(t - \Delta t) - 2H(t - 2\Delta t) + H(t - 3\Delta t)$. We also observe that the jumps in each of these perturbed step pulses are the result of and are directly proportional to the changes in gradient with respect to time in the original exciting triangular pulses.

An interesting phenomenon, that can be observed in the third time step $t = 3\Delta t$, is that the stress pulse reaches a level which is larger than unity—the magnitude of the self-effect (see time step $t = \Delta t$ at $y = 0$). Physically, this implies that the displacement discontinuity element can achieve a larger stress influence on an element located at $y > 0$ than the stress influence that the element has on itself. This situation arises from the interference of the diffracted pulses that emanate from the singular points at the edges of the element. We shall refer to these large stress regions as persistent diffracted pulses. As the stress wave moves further away from the displacement discontinuity element, the width of the portion of the pulse that does not decay decreases. The width of this region is determined by the difference between the distance travelled by the signal that begins at the centre of the element and that travelled by the signals that begin at the edges of the element.

In order to measure the effect that these persistent diffracted pulses have on the stability properties of displacement discontinuity algorithms, we consider the special case of two parallel displacement discontinuity elements of length $2\Delta x$ separated by a distance h shown in Figure 1. In this case the matrix problem (11) involves a 2×2 matrix

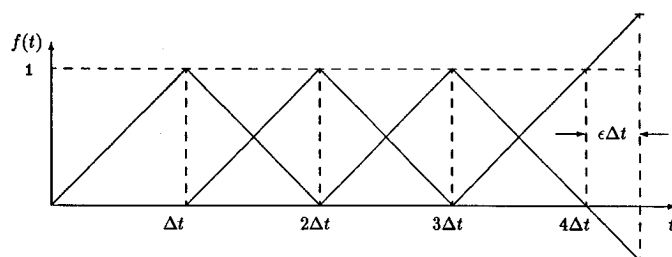
$$\mathbf{C}(z) = \begin{pmatrix} a_0 + a_1/z + \dots & b_0 + b_1/z + \dots \\ b_0 + b_1/z + \dots & a_0 + a_1/z + \dots \end{pmatrix} \tag{20}$$

$$= \begin{pmatrix} a(z) & b(z) \\ b(z) & a(z) \end{pmatrix} \tag{21}$$

and the stability condition (15) reduces to the form $a(z)^2 - b(z)^2 = 0$ or $a(z) \pm b(z) = 0$.

From the above discussion of the persistent diffracted pulses, we expect that the regions where the remote influences are larger than the self-effect are associated with poor stability. Thus, if we place the second element in one of these regions then we would expect the resulting two-element problem to be unstable. In each plot of Figure 5 the magnitude of the largest root of the stability polynomial is represented as a function of the location y along the centre-line of the displacement discontinuity element at which the second displacement discontinuity element is placed (see the dashed line). Superimposed on these plots are the appropriate persistent stress waves due to the displacement discontinuity element which is located at the origin. We observe, for time steps $t = 3\Delta t$ and $t = 4\Delta t$, the close correlation between the regions in which the diffracted stresses are larger than the self effect and the regions within which the two element problem will be unstable because the stability root is larger than unity.

If the time step is altered (either increased or decreased) then it is possible that, due to the relative locations of the elements, no persistent diffracted pulse passes through the second element.

Figure 7. Basis functions for the ε -scheme

In this case the algorithm will most likely be stable because the self-effect will dominate all the influences over the time history of the model. This is the source of the intermittent instability phenomena that are observed in more complex displacement discontinuity models such as the Hook problems considered in Reference 18 and later in this section. Because the instability regions and the places where the persistent diffracted pulses occur are not identical, it is not possible to derive a simple criterion for instability based on the location of the persistent diffracted pulses. In addition, in problems with more complicated geometries the net effect of the persistent diffracted pulses may be difficult to assess—for example, when there are two lines of elements that are not parallel. It is for this reason that we have developed the more global stability checking procedures which we considered in Section 3.

It is interesting to note that if more than two of these parallel elements were stacked on top of one another, and their relative distances were chosen so that each one fell on a persistent diffracted pulse of one of the others, then we would be able to generate a numerical model which goes unstable extremely rapidly.

4.2. The enhanced stability of the ε -scheme

It is natural to try to consider possible remedies to the persistent diffractive pulses by considering other discretization schemes. In this subsection we consider the ε -scheme which was successful in the case of the modal model problem and the one-dimensional wave models considered in Reference 9. For the Hook problem considered in Reference 18 there is evidence that the ε -scheme improved the stability of the displacement discontinuity models. However, when subjected to the extreme situation presented by the two-element model problem, similar sorts of instabilities can be observed. In this section we determine the reason for the improved stability properties of the ε -scheme and the reason why it ultimately fails to resolve the two-element problem.

When the ε -scheme (whose basis functions are shown in Figure 7) is implemented in a constant/linear displacement discontinuity algorithm, similar persistent wave fronts are observed as is shown in Figure 8. The reason why the ε -scheme is more stable is that the diffraction from the tips of the element has the effect of increasing the self-effect while the persistent diffraction pulses are not increased. This has the net effect of improving the stability properties of the algorithm. However, the increase in the self-effect is not sufficient to remove the instabilities completely because some influences are still larger than the self-effect. The ε -scheme can be interpreted as a perturbation to the Trapezoidal scheme which provides improved stability characteristics. The stability often improves as the value of the parameter ε is increased, however, this gain in stability is off-set by an associated loss in accuracy. If ε is small the loss in accuracy is not noticeable, however, for $\varepsilon \approx 1$ a significant error in the form of a phase shift in the solution is observed.

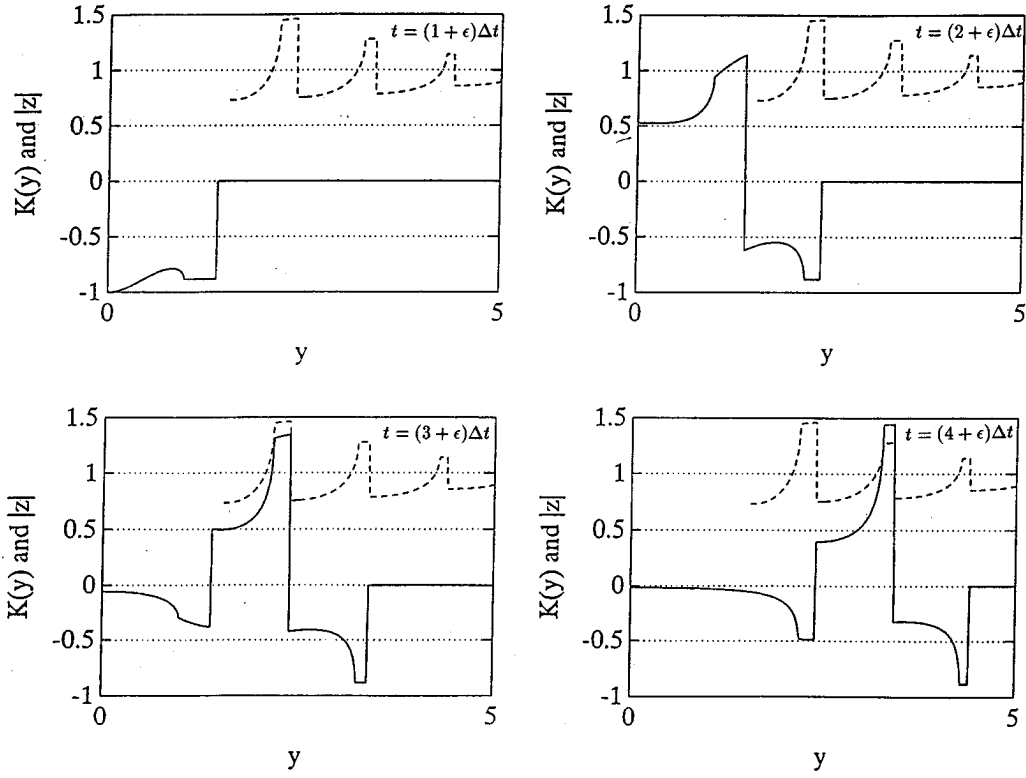


Figure 8. Regions of instability and the persistent wave fronts for the ϵ -scheme applied to the two element model problem

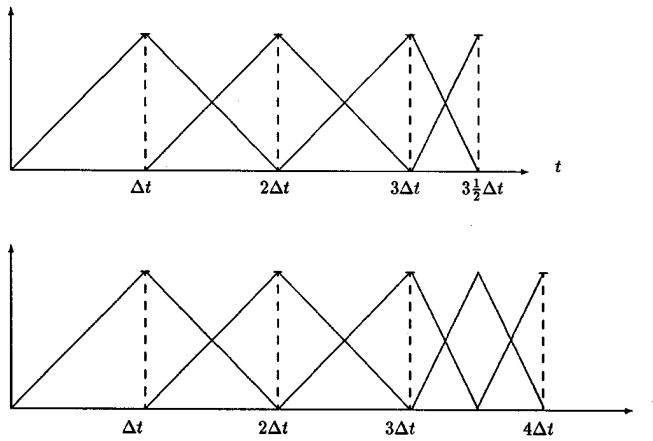


Figure 9. Basis functions for the half-step scheme (top) and full-step scheme (bottom)

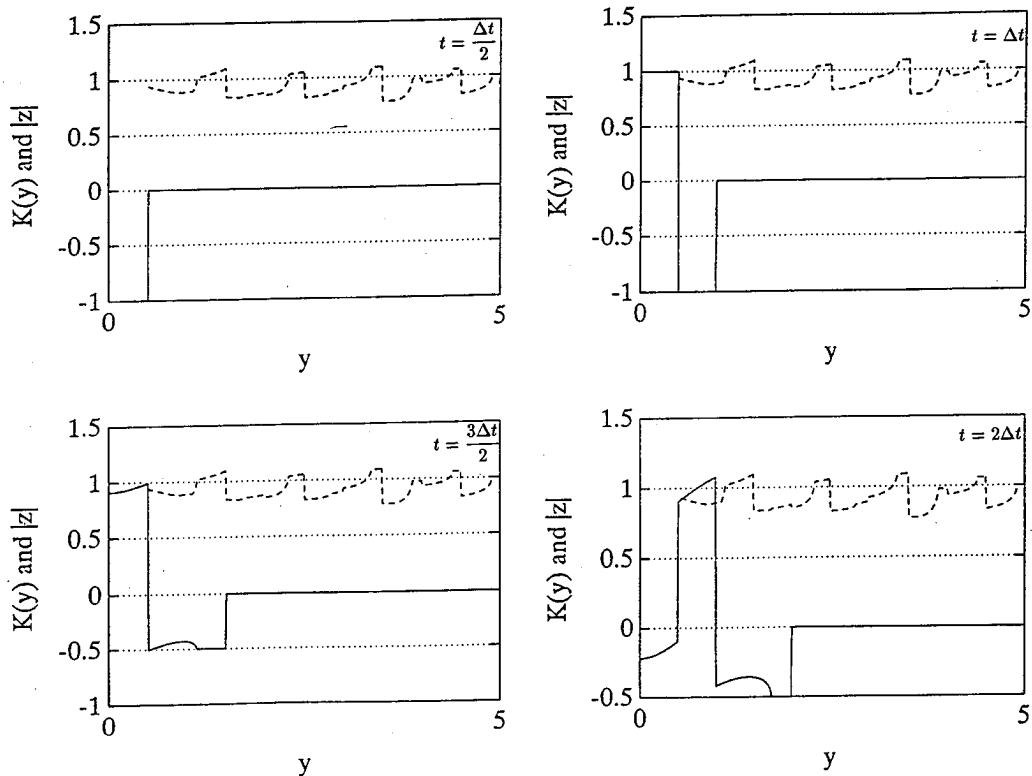


Figure 10. Regions of instability and the persistent wave fronts for the half-step scheme applied to the two element model problem for $t = \Delta t/2$ to $t = 2\Delta t$

4.3. The half-step scheme

The strategy for designing a new algorithm with improved stability properties must be to increase the self-effect while not increasing the magnitudes of the persistent diffraction pulses. The scheme we consider in this section exploits the relationship between the changes in gradient of the time basis functions and the jumps in the wave fronts in order to achieve improved stability properties.

4.3.1. Design and formulation. We have observed that the persistent wave fronts associated with the triangular basis functions of the piecewise linear displacement discontinuity method have jumps that are proportional to the changes in gradient of the basis functions. In order to achieve a large self-effect our idea is to start with a basis function with a large gradient and then change the basis functions to the standard piecewise linear triangles. The transition between basis functions should be such that the basis functions are consistent (i.e. they should all add up to unity so that they can at least model a constant function).

The solution is advanced in a sequence of two half-steps each of magnitude $\frac{1}{2}\Delta t$, while the convolution, which forms the major part of the computational burden, is performed using steps of magnitude Δt . In Figure 9 the basis functions associated with the first half-step and the second half-step (or the so-called full-step) are shown.

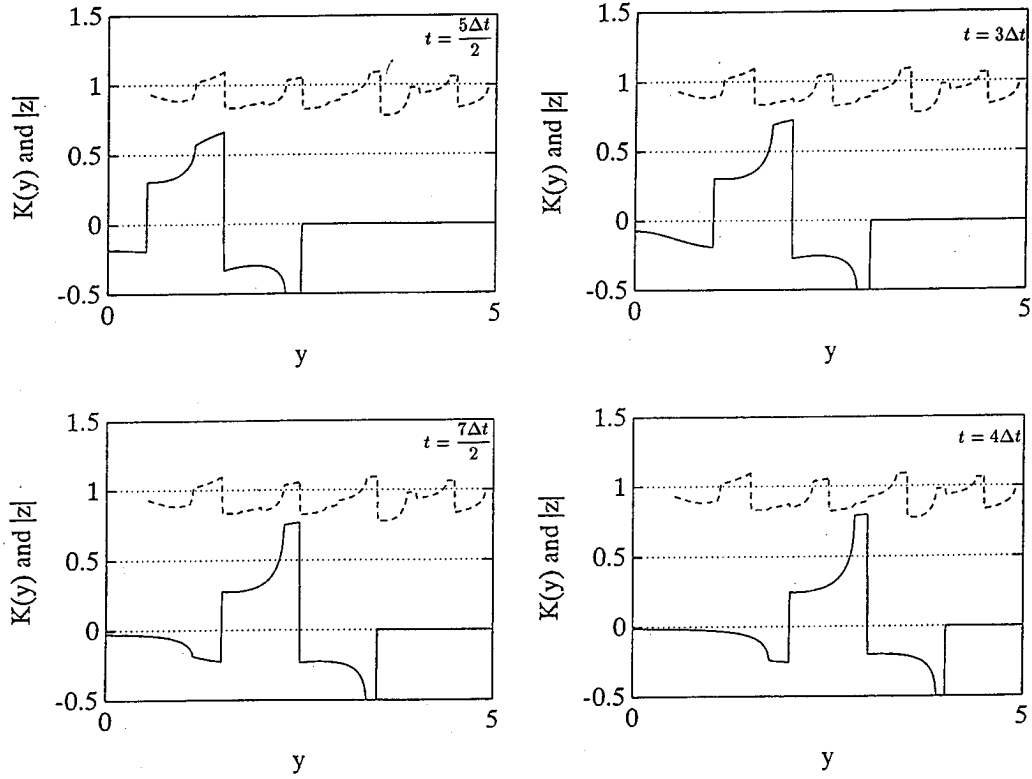


Figure 11. Regions of instability and the persistent wave fronts for the half-step scheme applied to the two element model problem for $t = 5\Delta t/2$ to $t = 4\Delta t$

The recursion for the half-step scheme can be expressed in the following form:

$$\begin{aligned} \mathbf{C}_0^h \mathbf{F}_{2m-1} + \sum_{k=0}^{m-1} \mathbf{C}_{2m-1-2k}^h \mathbf{F}_{2k} &= \mathbf{b}_{2m-1} \\ \mathbf{C}_0^f \mathbf{F}_{2m} + \mathbf{C}_1^f \mathbf{F}_{2m-1} + \sum_{k=0}^{m-1} \mathbf{C}_{2m-2k}^f \mathbf{F}_{2k} &= \mathbf{b}_{2m} \end{aligned} \quad (22)$$

where 'h' and 'f' imply half and full steps, respectively. In order to interpret this scheme in the same form as (10), we eliminate \mathbf{F}_{2m-1} from the full-step equation using the half-step equation in (22) to obtain

$$\mathbf{C}_0^f \mathbf{F}_{2m} + \sum_{k=0}^{m-1} \tilde{\mathbf{C}}_{2m-2k}^f \mathbf{F}_{2k} = \tilde{\mathbf{b}}_{2m} \quad (23)$$

where $\tilde{\mathbf{C}}_{2m-2k}^f = [\mathbf{C}_{2m-2k}^f - \mathbf{C}_1^f \mathbf{C}_0^{h-1} \mathbf{C}_{2m-1-2k}^h]$ and $\tilde{\mathbf{b}}_{2m} = \mathbf{b}_{2m} - \mathbf{C}_1^f \mathbf{C}_0^{h-1} \mathbf{b}_{2m-1}$. The stability analysis developed earlier in this section can now be applied to (23).

In Figures 10 and 11 we superimpose the plots of the half-step wave fronts (normalized with respect to the self-effect) and the magnitude of the zero of the stability polynomial with the largest modulus. We observe that the persistent wave fronts that plagued the Trapezoidal scheme are

now all less than the self-effect. Unfortunately, due to the modified recursion (23), there are still regions within which the maximal stability root is larger than unity. We observe that these regions of instability coincide with the basis functions that span two time steps and which are used to perform the convolution at the half-steps, i.e. those associated with the influence coefficients $C_{2m-1-2k}^h$, $k = m - 2, m - 3, \dots$. The effect of these basis functions is amplified by the factor $C_1^f C_0^{h-1}$ by which they are multiplied in (23). We refer to these basis functions as the shadow basis functions. Because of the regions of instability caused by the shadow basis functions for this two-element test problem, stability is not guaranteed for this new algorithm. However, this two element problem is somewhat extreme. Because the self-effect for the half-step scheme is double that of the Trapezoidal scheme we would expect that the half-step scheme would be more stable in general. Evidence of this enhanced stability is demonstrated for Hook problems in the next subsection.

4.3.2. Performance of the half-step scheme. Implementing the half-step scheme (22) requires significant modifications to the normal time-marching algorithm (10). The new basis functions that are needed to calculate the influence coefficients at each time step for the half-step scheme are shown in Figure 9.

The time step Δt (for each half-step) in the new algorithm (22) is taken as half the time step used in the old algorithm (10). This implies that twice as many time steps are needed to advance the solution to the same time horizon. The number of coefficient matrices that are required in the new algorithm is twice that required by the old algorithm. However, the number of calculations that are required does not increase accordingly because of the structure of the new algorithm. The largest share of CPU time is taken up by the calculation of the convolution histories at each time step, and this operation is only slightly slower for the new scheme than in the old scheme (even though there are twice the number of steps). Computer run times increase by about 50 per cent, but accuracy and stability are substantially improved. Because of the increased accuracy of the new scheme it is possible to use larger time steps. This implies that the new scheme is competitive with the old one (e.g. compare the run times of the two 150 time step runs in Table I). Table I compares the CPU times of the two schemes for different numbers of time steps. These results were obtained for the 28 element plane strain constant/linear Hook problem (see Figure 12) run on a Pentium 66 MHz machine. Figure 13 shows solutions obtained using the two schemes plotted against results from the ABAQUS/EXPLICIT¹⁹ finite element code. The half-step solution agrees well with the ABAQUS solution and is clearly more accurate and more stable than the Trapezoidal scheme.

Figure 14 shows the Hook problem results obtained from the linear/linear plane strain version of TWO4D with $Q1 = 0.6$, and a numerical instability is evident by 500 time steps. The stability analysis predicts two poles. Figure 15 shows the half-step results to 3000 time steps and there is no sign of an instability.

Further details of the implementation of this new algorithm as well as its application to other boundary element formulations are discussed in another paper.¹⁸

Table I. Run times for Trapezoidal versus half-step scheme

Time-stepping scheme	No. steps	Run time	Q1	Stable?
Trapezoidal	75	2.05 min	1.2	No
	150	6.23 min	0.6	Yes
	300	20.93 min	0.6	No
Half-step	150	3.30 min	1.2	Yes
	300	9.88 min	0.6	Yes

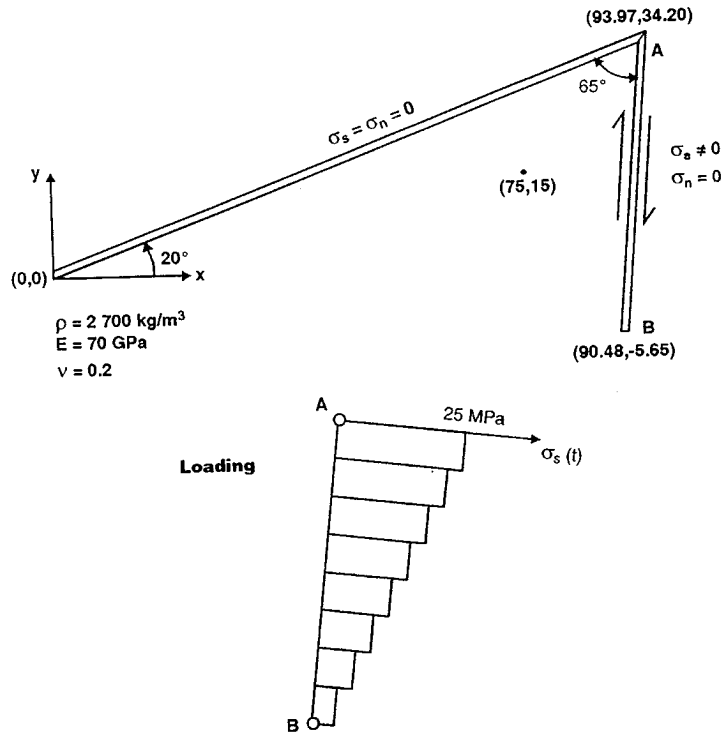


Figure 12. Plane strain Hook problem geometry which exhibits instabilities

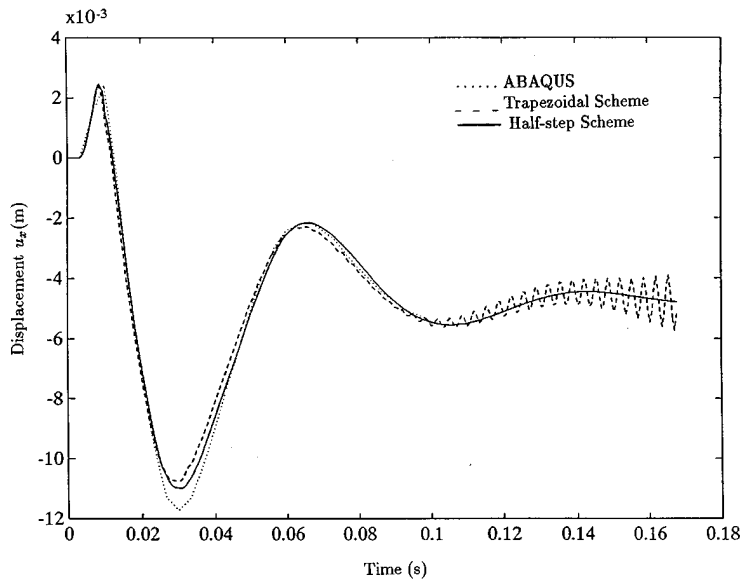


Figure 13. Standard, half-step, and ABAQUS/EXPLICIT results for Hook problem

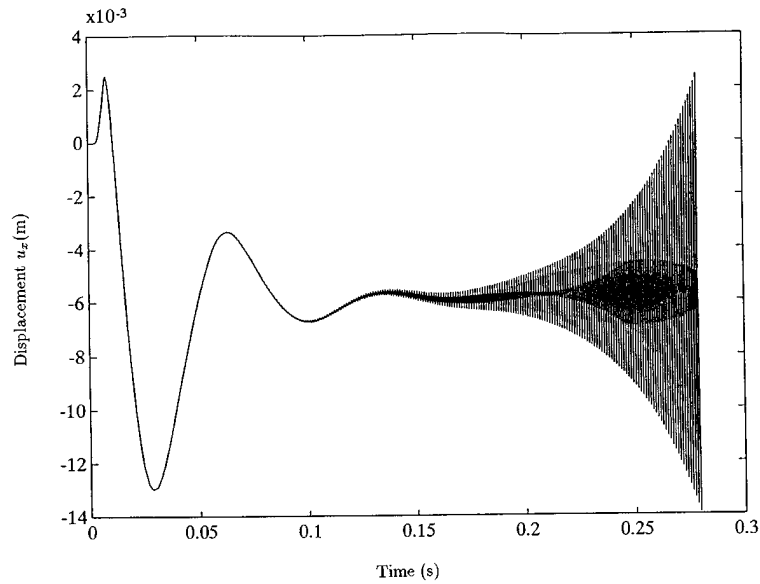


Figure 14. Standard linear/linear Hook problem, showing numerical instability

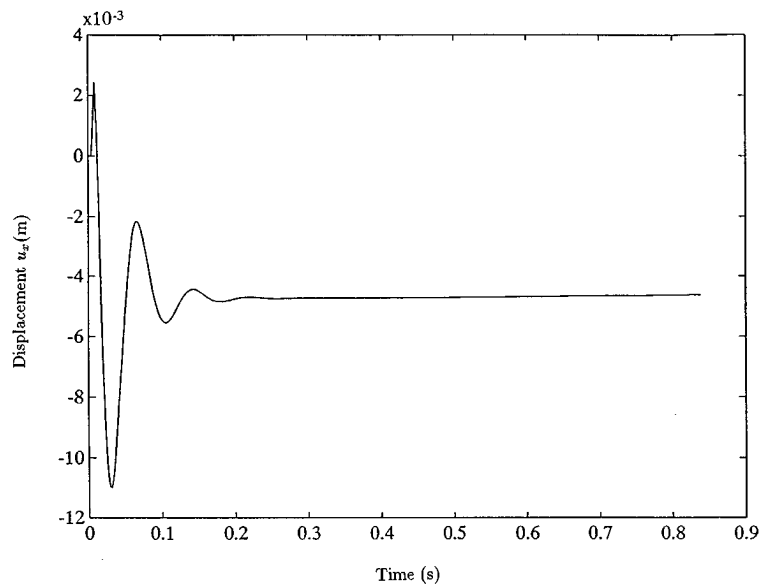


Figure 15. Half-step constant/linear Hook problem to 3000 time steps

5. CONCLUSIONS

Amid the growing evidence of numerical instabilities in boundary element elastodynamic models, there has hitherto been little theoretical investigation of the causes of these instabilities and the possible strategies for remediation. Up till now the user of a time-domain BE algorithm has no

way to guarantee *a priori* that a model with a given selection of meshing parameters will be stable. Indeed, there has been considerable frustration expressed in the literature¹ regarding the lack of predictability and alternative time-stepping procedures.

The objective of this paper has been to address this lack of theory. In this paper we generalized the stability theory established for model problems⁹ so that it can be applied to any time-domain boundary element algorithm. We showed that the stability of a given time-stepping scheme can be determined by finding the zeros of the characteristic determinant of the problem. Since each of the elements in the determinant is an infinite series, the determinant itself is also an infinite series. Thus, determining the roots (of which there are possibly an infinite number) of the stability determinant directly poses a formidable task. We outlined a methodology for approximating the stability determinant by a polynomial whereby the neglected roots are close to zero and therefore do not affect the stability of the method. Rather than searching for all the roots of this polynomial we developed a procedure, based on the Argument Principle, to check for the presence of unstable roots alone. We outlined practical procedures to implement the search for the presence of unstable roots.

Because of the potential for dynamic fracture modelling by means of the displacement discontinuity method, we used these stability analysis tools to investigate the sources of the instabilities in the displacement discontinuity method. To focus on the causes of these instabilities, we identified a simple example involving two parallel displacement discontinuity elements which rapidly exhibits potential instabilities. This test problem enabled us to establish the link between the persistent elasticity solutions, characteristic of displacement discontinuity elements, and the onset of exponential instabilities. In two dimensions an excited element will radiate a pulse which does not decay with distance from the source element. Indeed, as is the case for the model problems analysed in Reference 9, the stability of the problem is dominated by the relative magnitude of the effect that the element has on itself and the effect it has on its neighbours. Due to diffraction of the pulse caused by a change in the spatial variation of the displacement discontinuity, it is possible for the stress effect remote from an element to be larger than the effect that the element has on itself. This positive feedback between the two elements results in the instability. By appropriately changing the discretization procedure we showed that it is possible to develop new time-stepping schemes for the displacement discontinuity method with enhanced stability characteristics. We used this information to design a novel scheme, which we called the half-step scheme, with improved stability characteristics and greater accuracy for similar computational effort.

In summary, we have highlighted the causes of numerical instabilities in elastodynamic boundary element schemes, and have suggested a new algorithm—the half-step scheme, which delays and in some cases eliminates these instabilities. Furthermore, we have developed a numerical procedure which can be used to check *a priori* whether a particular problem will go unstable or not. We hope that the framework established in this paper will assist researchers in the assessment of the stability characteristics of their boundary element codes. We also hope that this paper will stimulate the development of new time-stepping algorithms that will enable dynamic boundary element algorithms to reach their full potential in practical applications.

ACKNOWLEDGEMENTS

The authors acknowledge the support of the Miningtek Laboratory of the Council for Scientific and Industrial Research of South Africa. The first author also acknowledges the support of the National Science and Engineering Research Council of Canada.

APPENDIX I

I.1. Discretization of ODE and boundary integrals

The relationship between the numerical solution of ordinary differential equations and the complications involved in the numerical solution of the dynamic boundary element equations can best be explained in terms of the following simple integral equation:

$$b(t) = \int_0^t K(t-s)f(s) ds = \int_0^t f(s) ds \quad (24)$$

This is a trivial convolution equation similar to the type of time convolution integral equation of the first kind that needs to be solved in the dynamic boundary element formulations. In this case we have chosen the kernel $K(t-s) = 1$ whereas the dynamic boundary element equations involve a singular kernel and vector quantities. In this equation, we are given $b(t)$ and we need to determine $f(t)$. By differentiating (24) both sides we see that (24) is equivalent to the ordinary differential equation:

$$b'(t) = f(t) \quad (25)$$

To see what is involved when we try to solve the integral equation (24) (i.e. find $f(t)$ given $b(t)$) we can look to the ordinary differential equation (25). We essentially need to perform the process of numerical differentiation because given $b(t)$, we need to determine $b'(t) = f(t)$. This is a notoriously ill-conditioned process. In contrast, when solving the ordinary differential equation (25) we are typically given $f(t)$ and we need to determine $b(t)$ —this amounts to numerical integration which is much better conditioned. In fact (24) provides a representation for the solution $b(t)$ to the ordinary differential equation (25), which is a starting point for the derivation of many of the numerical schemes that are used to solve ordinary differential equations. For example, the trapezoidal approximation to the integral in (24) yields the Crank–Nicolson or Trapezoidal method to solve (25). Thus, similar discretization techniques can be used to solve the integral equation (24) and the ordinary differential equation (25). Indeed, various discretizations of the integral in (24) yield a variety of different schemes for solving the integral equation (24). Although the discretization strategies may be the same, the stability properties of the approximation scheme for the ordinary differential equation and the integral equation are very different. In particular, a discretization of (24) is of the form:

$$b_N = \Delta t \sum_{k=0}^N w_k f_k \quad (26)$$

Solving (25) involves evaluating the convolution sum on the known quantities f_k , whereas solving (24) using the same discretization involves *inverting* the convolution sum to find f_k given b_k .

APPENDIX II

II.1. The z-transform

Definition II.1 The z-transform of a causal sequence $\{f_k: f_k = 0 \text{ if } k < 0\}$ is defined to be

$$F(z) = Z[f_k] = \sum_0^{\infty} f_k z^{-k} \quad (27)$$

while the z -transform of a continuous function $f(t)$ with the sampling period Δt is defined to be:

$$F(z) = Z[f(k\Delta t)] = \sum_0^{\infty} f(k\Delta t)z^{-k} \quad (28)$$

Although there are many more, we only list some of the important properties of the z -transform that we need in our stability analysis that follows. These properties can be derived directly from the definition of the z -transform:

Property 1. (Linearity):

$$Z[\alpha f_k + \beta g_k] = \alpha Z[f_k] + \beta Z[g_k] \quad (29)$$

Property 2. (Backward shift):

$$Z[f_{k-m}] = z^{-m}Z[f_k] \quad (30)$$

Property 3. (Forward shift):

$$Z[f_{k+m}] = z^m \left\{ Z[f_k] - \sum_{k=0}^{m-1} f_k z^{-k} \right\} \quad (31)$$

Property 4. (Convolution):

$$Z \left[\sum_{m=0}^k f_{k-m} g_m \right] = F(z)G(z) \quad (32)$$

Property 5. (Inversion integral): Let C be a closed contour enclosing all the poles of $F(z)$ then:

$$f_k = \frac{1}{2\pi i} \int_C F(z)z^{k-1} dz \quad (33)$$

APPENDIX III

III.1. Truncating $\det(C(z))$ and stability zeros

In this appendix we consider the effect that the truncation procedure (16) has on the stability roots. The infinite series $\det(C(z))$ potentially has an infinite number of zeros, whereas the approximating polynomial $p_{MN}(z)$ has only MN zeros. We consider conditions under which it is possible to truncate the series without affecting the number of unstable zeros. Since, we are considering a search for only unstable zeros $|z| > 1$ of $\det(C(z))$ we explicitly exclude the case of marginally stable roots of $\det(C(z))$ which lie on the unit disk $|z| = 1$. The argument followed in this appendix is fairly common in complex analysis (see for example Reference 15) but will be presented in this appendix for the sake of completeness.

Let $MN = \mathcal{N}$ and consider the zeros of the polynomial

$$p_{\mathcal{N}}(z) = a_0 z^{\mathcal{N}} + a_1 z^{\mathcal{N}-1} + \cdots + a_{\mathcal{N}} \quad (34)$$

which is a truncation of $\det(C(z))$. In order to focus on the unstable zeros only, we consider the complimentary polynomial:

$$q_{\mathcal{N}}(z) = z^{\mathcal{N}} p_{\mathcal{N}} \left(\frac{1}{z} \right) = a_0 + a_1 z + \cdots + a_{\mathcal{N}} z^{\mathcal{N}} \quad (35)$$

of $p_{\mathcal{N}}(z)$. The conformal map $w = \frac{1}{z}$ associates the unstable zeros $|z| > 1$ of $p_{\mathcal{N}}(z)$ with the zeros of $q_{\mathcal{N}}(z)$ which lie within the unit disk $|z| < 1$. Provided the coefficients a_n of $q_{\mathcal{N}}(z)$ have the following asymptotic behaviour:

$$|a_n| \sim \frac{1}{n^p} \text{ as } n \rightarrow \infty, \text{ where } p > 1 \quad (36)$$

then, by the Weierstrass M-test, the sequence of partial sums $\{q_n\}$ converges uniformly within the unit disk $|z| \leq 1$ to the limit function $q(z) = \sum_{n=1}^{\infty} a_n z^n$. Since, we are only considering the unstable zeros $|z| < 1$ of $q(z)$, we assume that $q(z)$ has no zeros on the unit circle $C_1 = \{z : |z| = 1\}$. Since, $q(z)$ is analytic and therefore continuous on the compact set C_1 and non-zero on C_1 , there exists an $m_0 > 0$ such that $|q(z)| \geq m_0 > 0$. Since the sequence $q_n(z)$ converges uniformly to $q(z)$ on C_1 , there exists an integer N_0 such that

$$n \geq N_0 \Rightarrow |q_n(z) - q(z)| < m_0 \leq |q(z)| \text{ for all } z \in C_1 \quad (37)$$

Since, $q_n(z)$ and $q(z)$ are analytic on $|z| \leq 1$, it follows from Roché's theorem that each of the $q_n(z)$ for which $n \geq N_0$ have precisely the same number of zeros within C_1 as does $q(z)$.

Thus, provided the sequence of influence coefficients a_n converge sufficiently rapidly to satisfy (36), it is possible to truncate infinite series without compromising the stability analysis.

REFERENCES

1. D. J. Andrews, 'Dynamic growth of mixed-mode shear cracks', *Bull. Seism. Soc. Am.*, **84**, 1184–1198 (1994).
2. M. G. Mack, 'A three-dimensional boundary element method for elastodynamics', *Ph.D. thesis*, University of Minnesota, U.S.A., 1991.
3. E. Siebrits, 'Two-dimensional time domain elastodynamic displacement discontinuity method with mining applications', *Ph.D. thesis*, University of Minnesota, U.S.A., 1992.
4. Y. Tian, 'Boundary element method in elastodynamics', *Ph.D. thesis*, University of Minnesota, U.S.A., 1990.
5. M. C. Loken, 'A three-dimensional boundary element method for linear elastodynamics', *Ph.D. thesis*, University of Minnesota, U.S.A., (1992).
6. J. Dominguez, *Boundary Elements in Dynamics*, Computational Mechanics Publications, Southampton, 1993.
7. H. L. Selberg, 'Transient compression waves from spherical and cylindrical cavities', *Arkiv for Fysik*, **5**, 97–108 (1951).
8. M. G. Koller, M. Bonnet and R. Madariaga, 'Modelling of dynamical crack propagation using time-domain boundary integrals', *Wave Motion*, Vol. 16, 339–366 (1992).
9. A. P. Peirce and E. Siebrits, 'Stability analysis of model problems for elastodynamic boundary element discretizations', *Numer. Methods for Partial Differential Equations*, to appear.
10. S. Kobayashi, 'Fundamentals of boundary integral equation methods in elastodynamics', in Brebbia (ed.), *Topics in Boundary Element Research, Vol. 2: Time-dependent and vibration problems*, Springer, New York, 1985, pp. 1–54.
11. P. K. Banerjee, S. Ahmad and G. D. Manolis, 'Advanced elastodynamic analysis', in (ed. Beskos), *Boundary element methods in mechanics*, 1987, pp. 258–284.
12. K. Ogata, *Discrete-time Control Systems*, Prentice-Hall, Englewood Cliffs, N.J., 1987.
13. L. Sirovich, *Introduction to Applied Mathematics*, Springer, New York, 1988.
14. R. V. Churchill and J. W. Brown, *Complex Variables and Applications*, McGraw-Hill, New York, 1988.
15. J. E. Marsden and M. J. Hoffman, *Basic Complex Analysis*, 2nd edn., Freeman, New York, 1987.
16. W. H. Press, S. A. Teukolsky, W. T. Vetterling and B. P. Flannery, *Numerical Recipes*, 2nd edn., Cambridge University Press, New York, 1992.
17. L. B. Freund, *Dynamic Fracture Mechanics*, Cambridge University Press, Cambridge, 1993.
18. E. Siebrits and A. P. Peirce, 'Implementation and application of elastodynamic boundary element discretizations with improved stability properties', *Int. J. for Computer-aided Eng. & Software* (submitted).
19. HKS (Hibbitt, Karlsson, and Sorensen, Inc.), *ABAQUS/EXPLICIT version 5.3-1*, Rhode Island, 1994.
20. A. C. Eringen and E. S. Suhubi, *Elastodynamics: Vol. II Linear Theory*, Academic Press, New York, 1975.
21. A. E. Love, *A Treatise on the Mathematical Theory of Elasticity*, Dover, New York, 1944.
22. G. G. Stokes, 'On the dynamical theory of diffraction', *Trans. Cambridge Phil. Soc.*, **9**, 1–62 (1849).
23. A. N. Tikhonov and Y. Y. Arsenin, *Solutions to Ill-posed Problems*, Winston-Wiley, New York, 1977.